Pergamon

Acta Materialia 50 (2002) 1063–1073

Acta MATERIALIA

www.actamat-journals.com

Large deformation simulations of cyclic displacement instabilities in thermal barrier systems

M.Y. He [a,*], J.W. Hutchinson [b], A.G. Evans [c]

[a] *Materials Department, University of California, Santa Barbara, CA 93106-5050, USA*
[b] *Division of Engineering and Applied Science, Harvard University, Cambridge, MA 02138, USA*
[c] *Princeton Materials Institute, Princeton University, Princeton, NJ 08540, USA*

Received 15 August 2001; accepted 18 October 2001

Abstract

The cyclic displacement instability exhibited by a thermally grown oxide (TGO) in a thermal barrier system has been simulated using a scheme that embodies large-scale thickening. The investigation has three main objectives. (i) A sensitivity study that probes the influence of the thermo-mechanical properties of the bond coat. It uses properties that closely resemble those relevant to actual bond coat materials. (ii) Explore the influence of the size of the imperfections present on the bond coat surface and address the critical size below which the instability is suppressed. (iii) A determination of the influence of TGO growth kinetics ranging between linear and parabolic. © 2002 Acta Materialia Inc. Published by Elsevier Science Ltd. All rights reserved.

Keywords: Physical vapor deposition (PVD); Thermal barrier systems; Computer simulation; Layered materials; Fatigue

1. Introduction

Thermal barrier systems used in gas turbines are tri-layers, comprising an alloy bond coat, an oxide thermal barrier coating (TBC) and a thermally grown oxide (TGO) [1–5]. Durability assessments have drawn attention to the importance of cyclic plasticity in the bond coat, through its governance of TGO displacement instabilities [6–9]. The most vivid manifestation is the periodic downward displacements of the TGO in a system with a Pt–allemande bond coat (β–NiAl with Pt in solution) that creates lateral cracks in the superposed TBC (Fig. 1) [6]. The effect is motivated by the combined influence of the thermal expansion misfit between the TGO and the substrate, as well as the growth strains in the TGO [6–11].

Earlier numerical simulations have demonstrated responses that duplicate the experimental trends [8,9]. However, because of numerical limitations, changes in the TGO thickness upon cycling have been limited to levels smaller than the initial thickness. This restriction has confined the scope to a small number of cycles conducted on pre-oxidized systems with a thin, initial TGO [8,9]. The present article establishes a procedure for incorporating finite thickening and focuses on its consequences. The simulations are performed for a bond coat hav-

* Corresponding author.
E-mail address: ming@engineering.ucsb.edu (M.Y. He).

PII: S1359-6454(01)00406-2

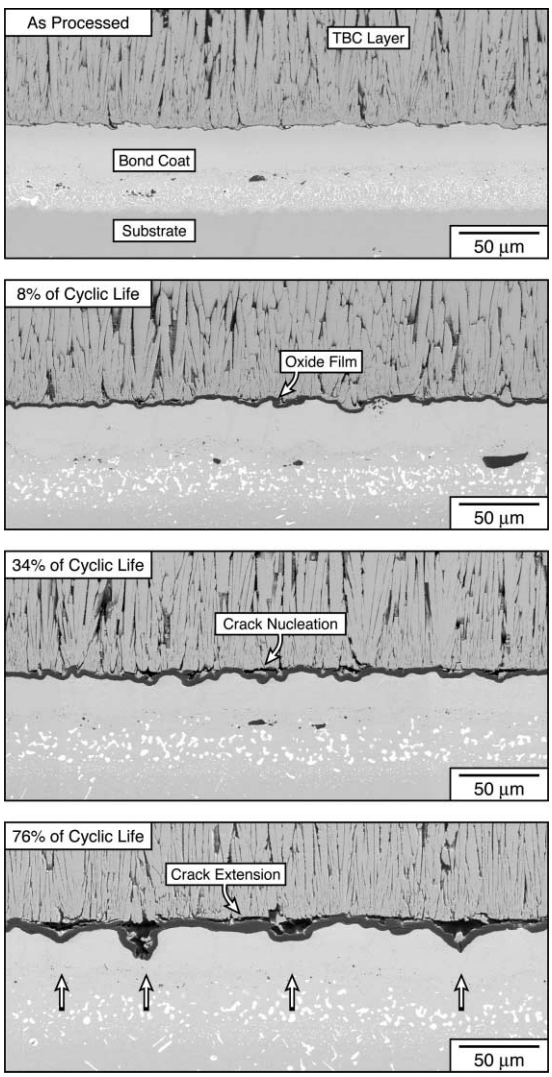

Fig. 1. The TGO displacement instability upon thermal cycling of a TBC system with a Pt–aluminide bond coat [6].

ing representative thermo-mechanical properties [9,12,13]. That is, the alloy has temperature-dependent yielding characteristics, as well as a thermal expansion misfit with the substrate [13].

By introducing features that closely resemble those applicable to actual bond coat systems, the origins of several effects observed in experiments [6,14] have been distinguished. These include the role of the bond coat mechanical properties as well as the influence of the size of the imperfections present on the bond coat surface, and the effect of TGO growth kinetics (linear relative to parabolic).

The ability to incorporate finite thickening enables another key aspect of the instability to be assessed. Namely, the influence of the amount of new TGO forming at the interface to cause thickening, relative to that forming on the internal grain boundaries that results in a growth strain, ε_g [1]. The latter allows the TGO to elongate at the instability [6].

2. The model

Two topological choices have been used in prior analyses: one for a surface having sinusoidal undulations (ridges and valleys), subject to plane strain [8], and the other for isolated, axi-symmetric undulations and protuberances [9]. The trends appear to be insensitive to this difference. The present simulations use the sinusoidal morphology. The TGO layer oscillates with amplitude A_0 and wavelength $2L$, varying as: $z = (A_0/2)\cos(\pi x/L)$ (Fig. 2), with $A_0/L = 0.6$ in all calculations.

Most of the concepts underlying the propagation of instabilities have been elaborated elsewhere [8,9,15] and are only summarized here for completeness. The TGO characteristics are explained first. The growth is simulated by a stress-free strain tensor applied at the maximum temperature [9,15]. Consistent with experimental findings [6,14], this strain has a small lateral component, ε_g, and a

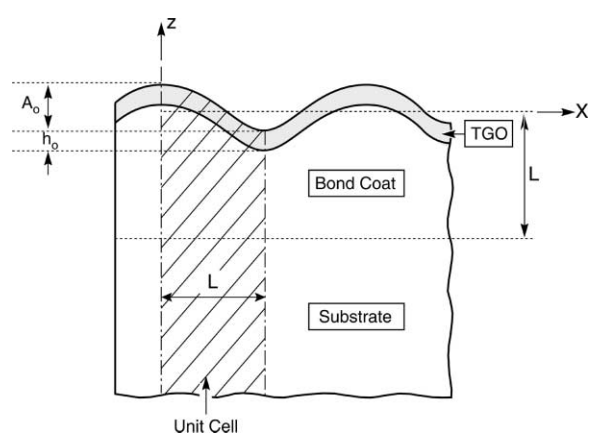

Fig. 2. A schematic of the configuration analysed.

larger thickening component, $\Delta h/h_0$. The thickening per cycle, Δh, is a variable, initially taken to be a fixed fraction, f, of the initial thickness, h_0. Subsequent simulations are performed with the parabolic thickening kinetics found experimentally [1,16]: whereupon the increment in thickness per cycle, subject to hot time, Δt, becomes:

$$\frac{\Delta h}{h-h_0} = \frac{\Delta t}{2t} \tag{1}$$

where t is the cumulative hot time.

Stress redistribution upon cycling is simulated by imparting the yield characteristics plotted in Fig. 3(a) [9,15]. That is, at the peak temperature, the TGO yields when the Mises stress reaches ±1 GPa, imposing a maximum on the growth stress [1,10]. On cooling and reheating it behaves elastically, because of the rapid increase in yield strength at lower temperatures. The stress at ambient then equals the sum of that from growth with that from thermal expansion misfit ($\sigma_{\text{ambient}} \approx -4.5$ GPa) [1,10].

The bond coat is considered next. It is taken to have a temperature-dependent yield strength having the form depicted in Fig. 3(b) [9,12]. The strength up to temperature T_1 (taken as 300°C in all calculations) is 1 GPa. At temperatures above T_2, the strength $\sigma_{Y\,\min}^{bc}$ is allowed to vary in the range of 50–200 MPa. It changes linearly from T_1 to T_2.

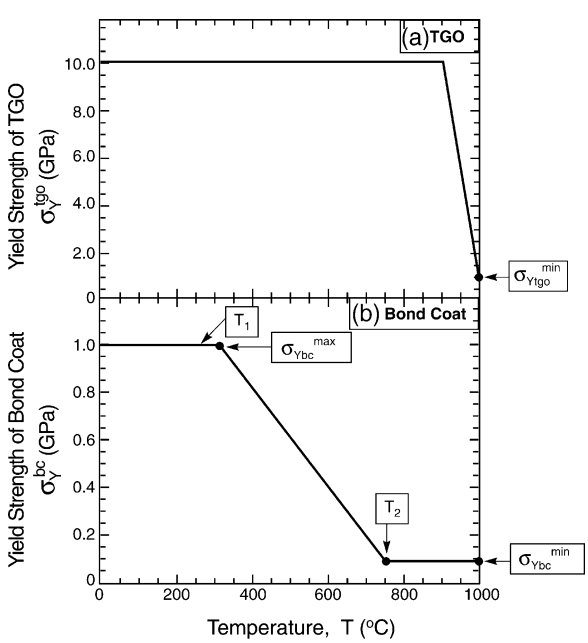

Fig. 3. The temperature-dependent yield strengths used for the simulations: (a) TGO, (b) bond coat [9].

Time-dependent (creep) effects are not addressed with this representation. They are being examined in a separate study [17]. The bond coat is assigned a thermal expansion misfit with the superalloy substrate. For most calculations it is taken as: $\Delta\alpha_s = +3$ ppm/°C ($\Delta\alpha_s = \alpha_{sub} - \alpha_{bc}$) [13,18].

The stresses in the substrate are sufficiently small that they never attain the yield strength [8,9], enabling an elastic representation to be used.

3. The finite element implementation

The simulations have been conducted by the finite element method, using the general-purpose code ABAQUS. The unit cell (Fig. 2) has been described elsewhere [8]. A typical mesh includes about 3600 10-node generalized plane strain elements, which account for the bi-axial nature of thermal loading. Periodic boundary conditions are imposed. The material properties are similar to those used previously ($E_{sub} = 200$ GPa, $\nu_{sub} = 0.3$, $E_{bc} = 200$ GPa, $\nu_{bc} = 0.3$, $E_{tgo} = 400$ GPa, and $\nu_{tgo} = 0.2$) [1,8,9,13]. The new feature is the sub-routine for simulating TGO growth occurring at the maximum temperature. The lateral component, $\Delta\varepsilon_{xx} = \Delta\varepsilon_{zz} = \varepsilon_g$, is incorporated by imposing a transformation strain to all elements in the TGO layer, taken to be uniform through the thickness. Non-uniformities set up stress (chemical potential) gradients that would be rapidly eliminated through matter redistribution by grain boundary diffusion. The thickening simulation requires a different strategy. A strain ε_t is imposed *on the row of the bond coat elements immediately adjacent to the* TGO. An engineering strain measure is used, such that the ratio of the new volume to the original volume in the row of elements experiencing oxidation is, $(1 + \varepsilon_t)(1 + \varepsilon_g)^2$. Since ε_g is typically small compared with ε_t, the relative volume change upon changing from the alloy host phase to the

oxide product phase is effectively ε_t [19,20]. Simultaneously, the properties of these elements are switched from those characteristic of the bond coat to those applicable to the TGO. To avoid numerical instability the properties are changed incrementally, in a linear manner, as the thickening is imposed. The chosen thickening rate dictates the dimensions of the elements that undergo oxidation. For example, when $\varepsilon_t = 1$, in order to realize a thickening per cycle, Δh, the thickness of those bond coat elements experiencing the transition would be $\Delta h/2$. Two user subroutines have been written to perform these adaptations. Unless stated otherwise, the following simulations use a strain ratio, $\varepsilon_g/(\Delta h/h_0) = 0.005$, suggested by experimental measurements for a system with a Pt–aluminide bond coat [6].

4. General responses

Preliminary results for small thickness changes [Fig. 4(b) and (c)] elaborate and embellish earlier results [8,9]. A plot of the maximum Mises stress induced in the bond coat during one cycle (cooling, reheating and TGO thickening), relative to its yield strength [Fig. 4(a)], reveals the range of the cyclic plastic deformation beneath the impression [region A in Fig. 4(a)]. Because of the expansion misfit, the entire bond coat yields on cooling, but zone B in Fig. 4(a) remains elastic on reheating. Within the cyclic domain (zone A), the stress plot [Fig. 4(b)] indicates temperatures at which yielding commences on cooling, $T_{\text{yield}}^{\text{start}}$, and then ceases, $T_{\text{yield}}^{\text{cease}}$, because of the rapid rise in yield strength below T_2 [refer to Fig. 3(b)]. It also shows the temperature, T_{reyield}, at which reverse yielding occurs on reheating. Note that the stress readjusts, by $\Delta\sigma_{\text{growth}}$, as the TGO thickens at the peak temperature, causing $T_{\text{yield}}^{\text{start}}$ to decrease in the second cycle. Thereafter, it remains invariant.

The maximum vertical component of the plastic strain in zone A, $\varepsilon_{zz}^{\text{pl}}$ [Fig. 4(c)], reveals a complementary feature. That is, the temperatures for yielding, its cessation and for re-yielding are again apparent. But also note that, in this zone, $\varepsilon_{zz}^{\text{pl}}$ increases on a cycle-by-cycle basis, such that the plastic strain at ambient becomes systematically larger. Such strain accumulation is an indicator of ratcheting [9,15].

The foregoing responses, as well as others, become more vivid when a larger TGO thickening rate is incorporated into the simulations. Large-scale thickening results pertinent to the issues outlined in Section 1 are summarized in the following sections.

5. Large-scale thickening

5.1. The lateral growth strain

Ascertaining the role of the lateral growth strain is crucial. To assess this, simulations performed for zero growth strain have been compared with those for strains in the range, $\varepsilon_g = 5\text{–}20 \times 10^{-4}$, all for the same thickening per cycle, $\Delta h/h_0 = 0.2$. The results plotted in Fig. 5 typify all of the cases explored. Namely, absent a growth strain, the amplitude change rate, $\mathrm{d}A/\mathrm{d}N$, systematically *decreases* over about five cycles to a low (almost zero) level. It never becomes precisely zero, reflecting the continuous thickening of the TGO. When a growth strain exists ($\mathrm{d}\Delta A/\mathrm{d}N$ *increases* over the first few cycles and reaches a steady state, $(\mathrm{d}\Delta A/\mathrm{d}N)_{\text{ss}}$ [Fig. 5(a) and (b)]. The growth strain appears to be necessary because it allows the TGO to lengthen as the imperfection amplitude increases. Note that when the ratcheting rate is normalized by the growth strain [Fig. 5(c)], $(\mathrm{d}\Delta A/\mathrm{d}N)_{\text{ss}}$ is similar for all cases.

Given the key influence of the growth strain, all of the following calculations are performed for $\varepsilon_g/(\Delta h/h_0) = 0.005$, except the results shown in Figs. 11 and 13.

5.2. Stresses

Plots of the stress components (σ_{yy}, σ_{zz}) during a thermal cycle reveal the basis for cyclic plasticity [Fig. 6(a)]. Variations in σ_{xx} are similar to σ_{yy}: this stress has been omitted from the plots for clarity of presentation. Moreover, only the key features are emphasized. Upon cooling, locations of type A (Fig. 3) that experience cyclic yielding develop σ_{yy} *compressions*, accompanied by σ_{zz} *tensions*, con-

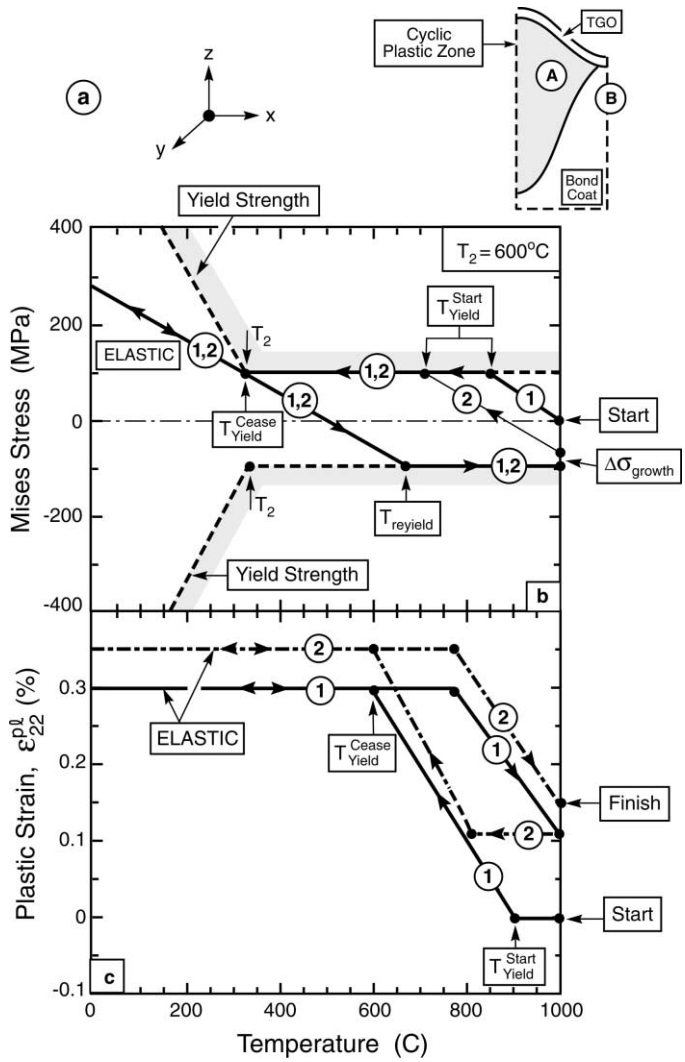

Fig. 4. (a) The regions of the bond coat that experience cyclic yielding (A) relative to those that yield only on cooling (B). (b) The change with temperature of the Mises stress in the bond coat, relative to the yield strength, for two thermal cycles, calculated at a location (site A) in the bond coat that experiences cyclic yielding. The temperatures at which yielding begins and ceases are indicated, as well as the reyield temperature. (c) The accumulation of plastic strain over 1.5 thermal cycles for the same location and conditions used to plot the stress depicted in Fig. 4(b) ($h_0/L = 0.08$, $A_0/2L = 0.3$, $\Delta h/h_0 = 0.2$, $T_2 = 600°C$, $\sigma^{min}_{Y\,bc} = 100$ MPa, $\varepsilon_g = 10^{-3}$).

sistent with established effects of thermal expansion misfit [1,19]. The deviatoric stresses, σ_e, being essentially the difference between σ_{yy} and σ_{zz}, are large, facilitating the plastic strain accumulation shown in Fig. 4. At locations outside this zone (region B in Fig. 3) *all of the stresses are compressive* [Fig. 6(b)] [1,19], such that the deviatoric stress is too small to cause reverse yielding.

The stresses readjust as the TGO thickens (Fig. 6). In the reverse yielding zone, A, all of the stresses increase upon thickening, whereas in zone B, they decrease.

5.3. Plastic strains

The plastic strain, ε^{pl}_{zz}, evolutions in zones A and B (Fig. 7) give some understanding of the consequences of the stresses. In this (and subsequent)

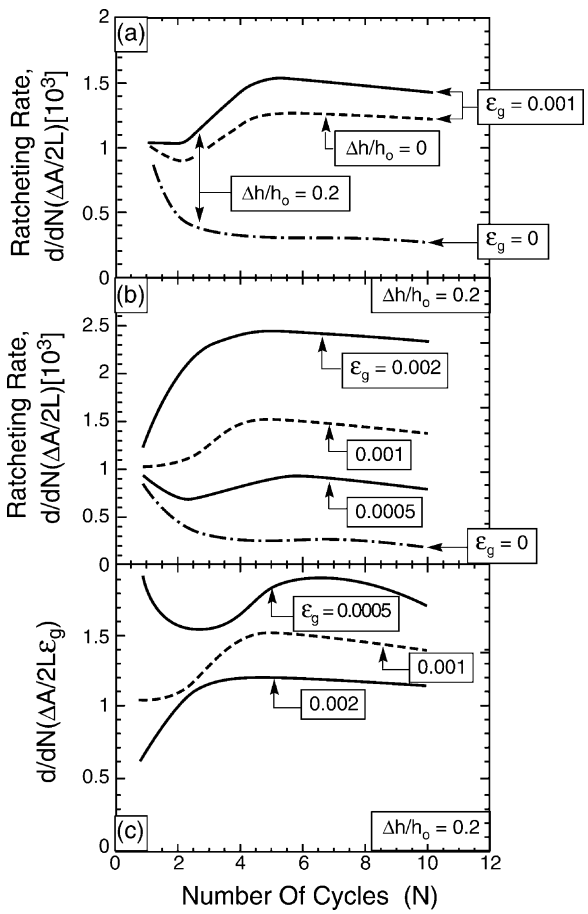

Fig. 5. The amplitude change rate subject to large-scale thickening. (a, b) A comparison of the response when the growth strain is zero and when finite, at fixed thickening per cycle. (c) The amplitude change per cycle normalized by the growth strain (when $\varepsilon_g > 0$) ($h_0/L = 0.08$, $A_0/2L = 0.3$, $\Delta h/h_0 = 0.2$, $T_2 = 600$°C, $\sigma^{\min}_{Y\,bc} = 100$ MPa).

figures, the abscissa refers to time steps t used in the numerical procedure. It relates to the cycling in the following manner. Each thermal cycle includes three steps: (1) cooling from 1000 to 0°C; (2) reheating from 0 to 1000°C; (3) TGO thickening and growth at 1000°C. In zone A, ε^{pl}_{zz} accumulates in each cycle, as the zone yields and re-yields, resulting in a cumulative upward displacement. There is no plastic strain during TGO growth, because the material beneath the TGO unloads elastically. In zone B, ε^{pl}_{zz} is an order of magnitude smaller and acts in the opposite direction, indicative of a small downward displacement. The strains occur primarily during TGO growth.

5.4. Amplitude changes

The amplitude changes, ΔA, are plotted in Figs. 8 and 9. A small increase in amplitude occurs isothermally, during TGO growth, ΔA_{growth}, highlighted in the inset, remaining invariant as the system cycles. A larger increase happens on cooling to ambient. It is non-linear down to T^{cease}_{yield} (Fig. 9), reflecting the development of plastic strains. Thereafter, the cooling is strictly elastic. On re-heating, because of elastic unloading, the amplitude decreases along the same path. There is a small non-linear domain above $T_{reyield}$ (Fig. 9). The consequence is a residual plastic displacement ΔA_{cycle}, highlighted in the inset (Fig. 8). Note that $\Delta A_{cycle} > \Delta A_{growth}$. On a cycle-by-cycle basis, the displacements continue to accumulate (Fig. 8). Effects of T_2 and $\Delta\alpha$ (Fig. 8) [9] indicate that the qualitative behavior is insensitive to the parameter selection.

Other results (Fig. 10) reveal that the cyclic amplitude change rate decreases as $\sigma^{\min}_{Y\,bc}$ increases [8,9].

6. Parabolic thickening

Modifications that arise when the TGO thickness increases in a parabolic (non-linear) manner [1,16] are addressed. The thickening law is that expressed by (1). Conducting such calculations requires a change to the input file for TGO thickening, with a corresponding change in the in-plane growth strain. Both growth strains, ε_g and $\Delta h/h_0$, are changed to assure that they remain proportional, $\varepsilon_g/(\Delta h/h_0) = 0.0375$. One set of results (Fig. 11) is typical. It compares the amplitude change rate, $d(\Delta A)/dN$, for linear and parabolic growth, all other aspects remaining invariant. The consequence is that, under parabolic conditions, the ratcheting rate diminishes on a cycle-by-cycle basis [Fig. 11(a)] instead of assuming a steady state. Note, however, that the amplitude change per increment in TGO thickness, $\Delta A/\Delta h$ [Fig. 11(b)], is essentially the same for both kinetic representations.

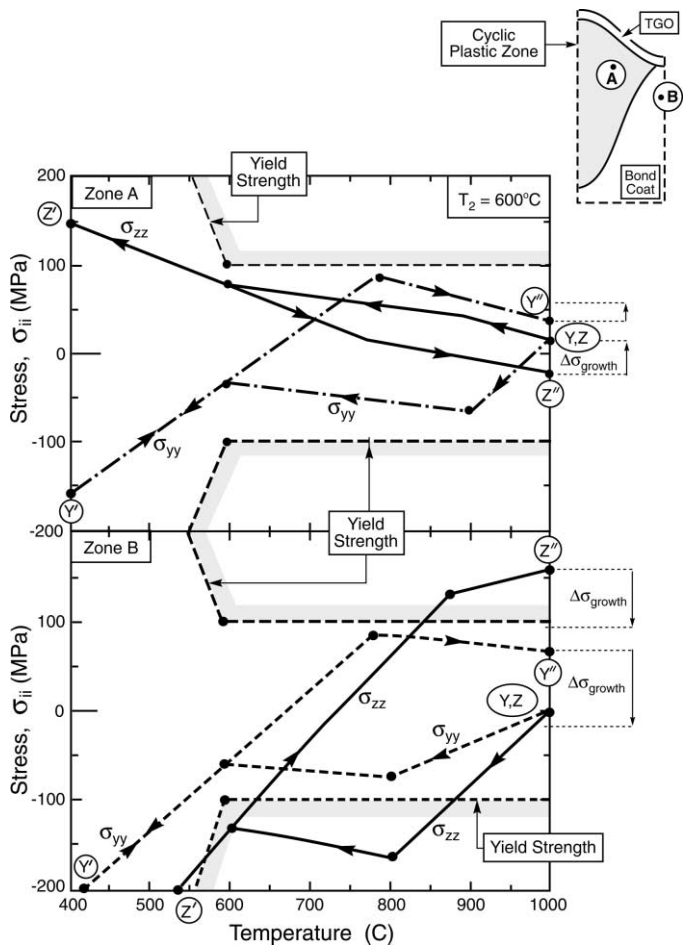

Fig. 6. Changes in the two components of the stress for a large-scale TGO thickening simulation. (a) In the region A subject to cyclic yielding and (b) the region B that yields only on cooling. Note that the σ_{zz} stress is tensile in region A, causing the Mises stress to increase rapidly as the temperature decreases ($h_0/L = 0.08$, $A_0/2L = 0.3$, $\Delta h/h_0 = 0.2$, $T_2 = 600$°C).

This trend mimics that measured experimentally (Fig. 12) [6]. Both experiment and simulation reveal that the ratcheting rate decreases by about a factor of three. Accordingly, the simulation establishes a direct connection between the ratcheting rate and the thickening kinetics of the TGO.

7. Imperfection size effect

To explore size effects, simulations have been performed for ratios of initial TGO thickness to undulation amplitude, h_0/A_0, between 0.1 and 4, all for fixed imperfection aspect ratio, $A_0/L = 0.6$, and for linear thickening ($\Delta h/L = 0.016$). The results are plotted in Fig. 13. As in all previous simulations, the growth rate, $\mathrm{d}(\Delta A)/\mathrm{d}N$ initially increases and then attains a steady state, $(\mathrm{d}\Delta A/\mathrm{d}N)_{ss}$, after about five cycles. Note from Fig. 13(b) that $(\mathrm{d}\Delta A/\mathrm{d}N)_{ss}$ decreases systematically *as the imperfection becomes smaller* (larger h_0/A_0). There is almost an order of magnitude decrease over the imperfection size range investigated. However, some ratcheting still occurs at the smallest size, $A_0/h_0 = 1/4$.

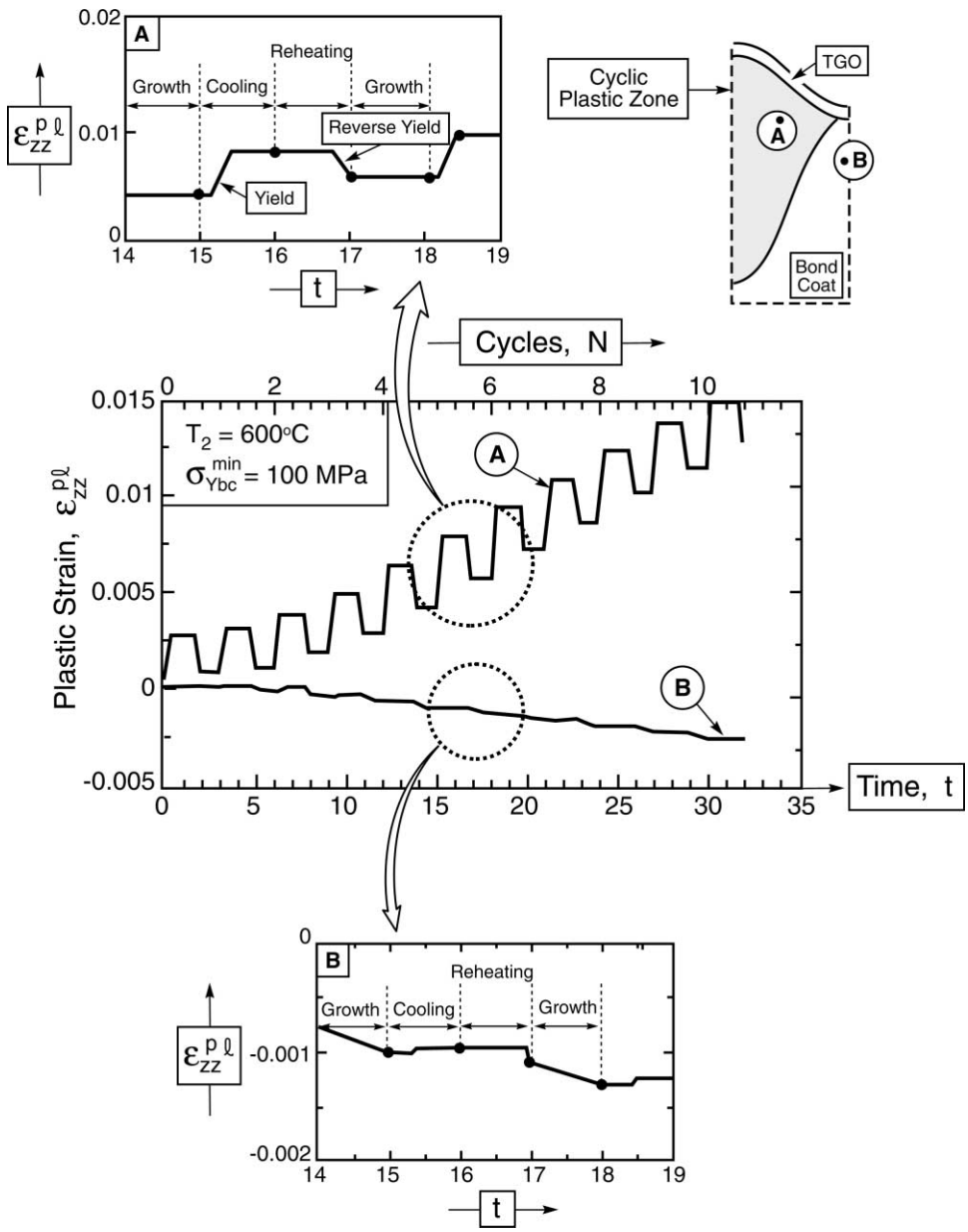

Fig. 7. The accumulation of the vertical component of the plastic strain, ε_{zz}^{pl} in regions A and B for the same conditions used to determine the stresses shown in Fig. 6. The temperatures/times at which the plastic strains arise are highlighted within the insets ($h_0/L = 0.08$, $A_0/2L = 0.3$, $\Delta h/h_0 = 0.2$, $T_2 = 600°C$, $\sigma_{Y\,bc}^{min} = 100$ MPa, $\varepsilon_g = 10^{-3}$). Here t refers to the time steps used in the numerical calculations: (1) cooling from 1000 to 0°C; (2) reheating from 0 to 1000°C; (3) TGO thickening and the growth at 1000°C.

8. Conclusion

By developing a sub-routine that allows instability simulations subject to large scale thickening of the TGO, four principal effects have been demonstrated.

(i) The calculations verify previous findings

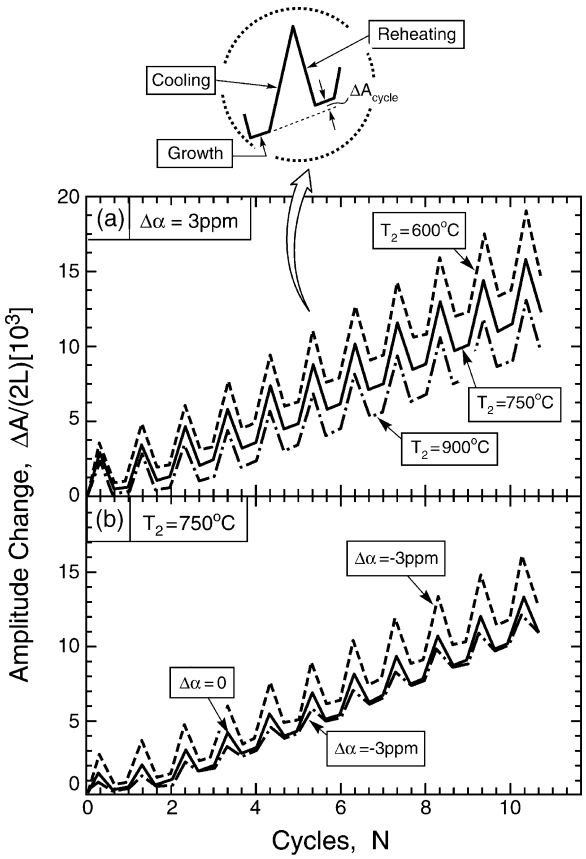

Fig. 8. The changes in imperfection amplitude that occur on a cycle-by-cycle basis for various choices of bond coat properties. The inset shows the amplitude change per cycle arising because of cyclic yielding, ΔA_{cycle} relative to that induced (isothermally) by TGO growth, ΔA_{growth} ($h_0/L = 0.08$, $A_0/2L = 0.3$, $\Delta h/h_0 = 0.2$, $\sigma^{min}_{Y\,bc} = 100$ MPa, $\varepsilon_g = 10^{-3}$).

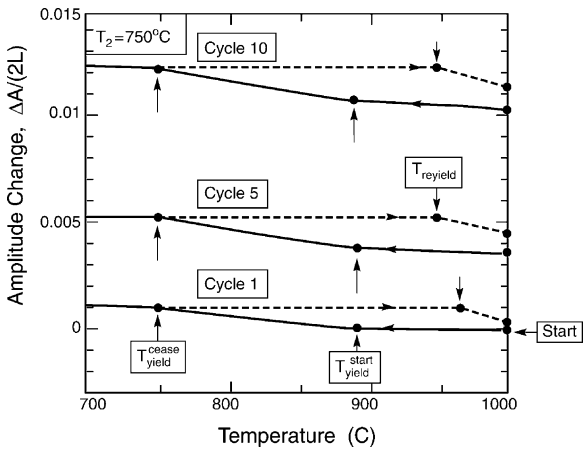

Fig. 9. Details of the amplitude changes shown in Fig. 8 for the first, fifth and tenth cycles ($h_0/L = 0.08$, $A_0/2L = 0.3$, $\Delta h/h_0 = 0.2$, $T_2 = 750$°C, $\sigma^{min}_{Y\,bc} = 100$ MPa, $\varepsilon_g = 10^{-3}$).

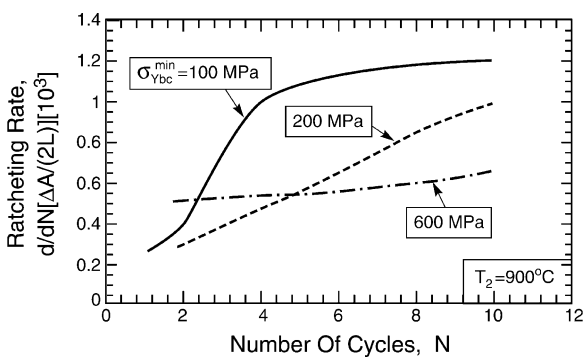

Fig. 10. The influence of the high temperature yield strength on the ratcheting ($h_0/L = 0.08$, $A_0/2L = 0.3$, $\Delta h/h_0 = 0.2$, $T_2 = 900$°C, $\varepsilon_g = 10^{-3}$).

[9] that a lateral growth strain is a necessary condition for continued cycle-by-cycle growth of the instability, because this strain allows the TGO to elongate with the bond coat as the imperfection amplitude increases.

(ii) The results also verify the earlier predictions [9] that the ratcheting rate is reduced by elevating the high-temperature deformation resistance.

(iii) A new finding is that there are substantial reductions in instability growth as the imperfection size approaches the thickness of the initial TGO layer. This prediction is consistent with the effect of surface planarization on instability development [14].

(iv) The calculations demonstrate that the ratcheting rate diminishes on a cycle-by-cycle basis when the TGO exhibits parabolic growth, contrasting with the steady-state that occurs when the growth is linear. The parabolic simulations are in accordance with experimental measurements [6].

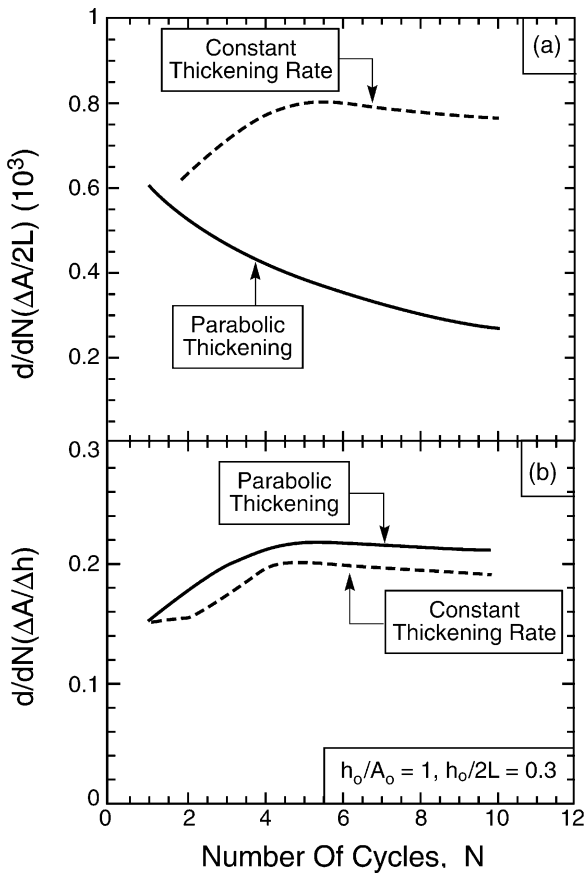

Fig. 11. (a) A comparison of the ratcheting rates for linear and parabolic TGO thickening. (b) The same results plotted as the amplitude change per TGO thickness increment, $\Delta A/\Delta h$ ($h_0/2L = 0.3$, $A_0/2L = 0.3$, $\Delta h/h_0/L = 0.016$, $T_2 = 750$°C, $\sigma_{Y\,bc}^{min} = 100$ MPa).

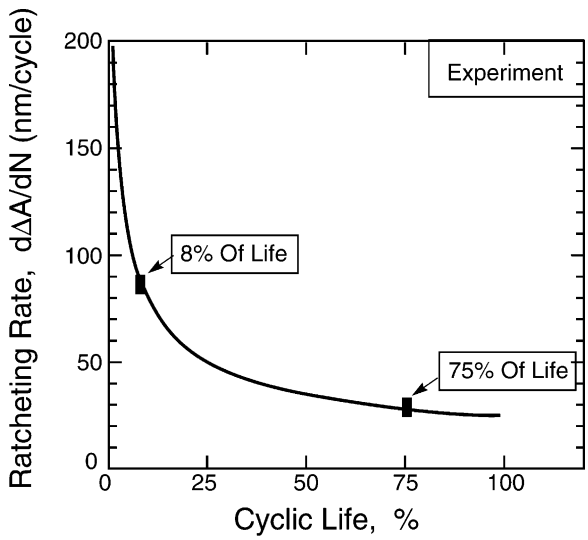

Fig. 12. Experimental measurements of the ratcheting rate for a TGO having parabolic growth characteristics [6].

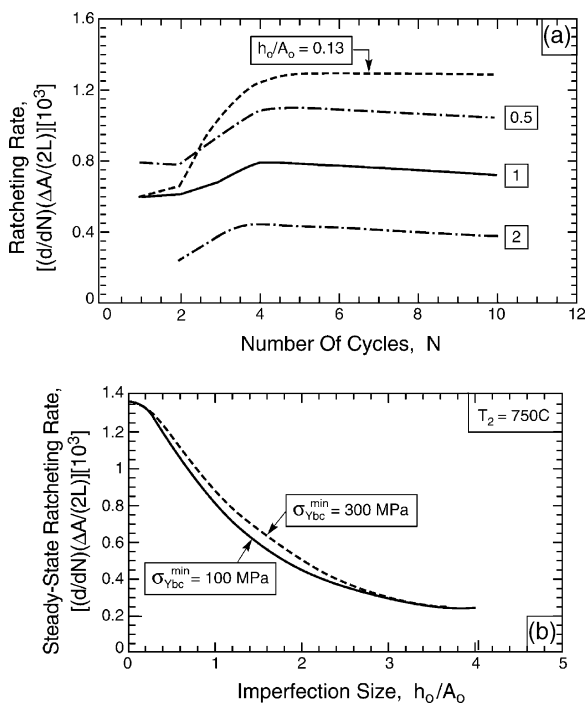

Fig. 13. Effects of the relative imperfection amplitude, A_0/h_0 on the ratcheting rate ($A_0/2L = 0.3$, $\Delta h/L = 0.016$, $T_2 = 750$°C, $\sigma_{Y\,bc}^{min} = 100$ MPa, $\varepsilon_g = 10^{-3}$).

Acknowledgements

The work was supported in part by the Office of Naval Research under ONR contract no. N00014-99-10170 and by the Advanced Gas Turbine Systems Research program of the Department of Energy under grant 01-01-SR093 through the South Carolina Energy Research and Development Center. Helpful suggestions by the reviewer are gratefully acknowledged.

References

[1] Evans AG, Mumm DR, Hutchinson JW, Meier GH, Pettit FS. Prog. Mater. Sci. 2001;46:505–53.
[2] Miller RA. J. Am. Ceram. Soc. 1984;67:517.
[3] Hillery R, editor. NRC Report, Coatings for high temperature structural materials. National Academy Press, 1996.
[4] Wright PK. Mater. Sci. Eng. 1998;A245:191–200.
[5] Strangman TE. Thin Solid Films 1985;127:93–105.
[6] Mumm DR, Evans AG, Spitsberg I. Acta mater. 2001;49:2329–40.
[7] Gell M, Vaidyanathan K, Barber B, Cheng J, Jordan E. Metall. Mater. Trans. 1999;30A:427–35.
[8] He MY, Evans AG, Hutchinson JW. Acta mater. 2000;48:2593–601.
[9] Karlsson AM, Evans AG. Acta mater. 2001;49:1793–804.
[10] Tolpygo V, Clarke DR. Acta mater. 2000;48:3283–93.
[11] Ambrico JM, Begley MR, Jordan EH. Acta mater. 2001;49:1577–88.
[12] Strangman TE. PhD Thesis, University of Connecticut, 1978.
[13] Hemker KJ. Unpublished results.
[14] Spitsberg I, Mumm DR, Evans AG. J. Mater. Res., in press.
[15] Karlsson AM, Levi CG, Evans AG. Acta mater., in press.
[16] Smialek JL, Jayne DT, Schaeffer JC, Murphy WH. Thin Solid Films 1994;253:285–92.
[17] Balint D, Hutchinson JW. Unpublished research.
[18] Watanabe M, Mumm DR, Chiras S, Evans AG. Scripta mater., 2002; 46: 67–70.
[19] Evans AG, He MY, Hutchinson JW. Prog. Mater. Sci. 2001;46:249–71.
[20] Rhines FN, Wolf JS. Metall. Trans. 1970;1:1701–5.